JOURNAL OF GEOPHYSICAL RESEARCH, VOL. 92, NO. C7, PAGES 7032–7044, JUNE 30, 1987

The Role of Shortwave Radiation in the Summer Decay of a Sea Ice Cover

GARY A. MAYKUT

Department of Atmospheric Sciences, University of Washington, Seattle

DONALD K. PEROVICH

U.S. Army Cold Regions Research and Engineering Laboratory, Hanover, New Hampshire

Heat balance models of ice, leads, and the underlying water column were used to investigate the role of shortwave radiation in the summer decay of a sea ice cover. Because of the potential importance of positive feedback between decreasing ice concentration and increasing solar input to the ocean, particular emphasis was given to the treatment of heat transfer and lateral melting in leads. The rate of heat loss to floe edges was calculated from lead temperatures using an empirical boundary layer parameterization. Coefficients for this parameterization were obtained from field measurements in the dynamically active ice cover of the Greenland Sea during the 1984 Marginal Ice Zone Experiment and in the static ice of Mould Bay, Northwest Territories. Field coefficients were found to be considerably larger than those previously obtained in the laboratory, suggesting that heat transfer rates near floe edges were controlled more by winds and currents than by local density differences. Model studies of individual leads indicate that heat losses to the atmosphere cause lateral melt rates to asymptotically approach a constant value as lead size increases. Thus although very wide leads transmit considerable energy to the underlying ocean, they have relatively little effect on lateral melting. Other results provide information on the relative importance of horizontal heat transfer rates, ice thickness, floe perimeter, atmospheric forcing, and oceanic heat flux. In general, the calculations indicate that much of the shortwave radiation entering the ocean is absorbed below the ice where it contributes to bottom ablation rather than lateral melting. This suggests that previous work has seriously overestimated the magnitude of the feedback between ice concentration and incident shortwave radiation.

INTRODUCTION

The summer decay and retreat of a sea ice cover is strongly influenced by the input of solar energy to the ice-ocean system. In regions of perennial ice where longwave radiation and the turbulent fluxes usually result in a net loss of heat from the surface, essentially all the energy needed to drive the melt cycle must be supplied by the incoming flux of shortwave radiation (F_r). Owing to more extensive melt pond coverage, seasonal ice in the Arctic basin generally absorbs even more shortwave radiation than the perennial ice and experiences correspondingly greater rates of surface ablation. Away from shore, decay patterns in seasonal ice are again controlled primarily by F_r. In coastal areas, however, the proximity of nearby land masses frequently results in the advection of warm air over the ice, and turbulent heat input to the ice can be significant. Measurements by *Langleben* [1966] indicate that sensible and latent heat fluxes in such regions can account for as much as 25% of the net energy gain by the surface. Near the free boundaries of the ice pack, incursions of warmer marine air can also produce periods during which the turbulent heat exchange is likely to be significant.

Heat input from the ocean is another important factor influencing the state and extent of the ice cover, particularly in the southern ocean and peripheral seas of the Arctic. Complicating efforts to quantify the relative importance of heat transport by the ocean is the discontinuous nature of the ice cover which allows large amounts of shortwave energy to enter the upper ocean through leads. In the Antarctic where surface ablation is small [*Andreas and Ackley*, 1982], the seasonal disappearance of the ice must be caused almost entirely by energy released from the water. *Gordon* [1981] estimates that up to 50% of this energy could be derived from water below the pycnocline, with the remainder presumably originating from shortwave radiation deposited in the upper ocean. The oceanic heat flux F_w in the central Arctic is about 2 W m^{-2} and has been shown to play a major role in determining the thickness of the perennial ice there [*Maykut and Untersteiner*, 1971]. The source of this heat was long believed to be the layer of relatively warm Atlantic water that occurs across much of the Arctic basin. More recently, however, it has been suggested that observed temperature changes in the Atlantic layer are largely due to mixing with colder shelf water [*Aagaard et al.*, 1981] and that F_w is determined almost completely by shortwave input through leads and areas of thin ice [*Maykut*, 1982]. In marginal areas such as the Greenland Sea, conditions are much more variable, and processes controlling transport of heat to the ice are not well understood. One of the principal goals of the recent Marginal Ice Zone Experiment (MIZEX) was to develop a quantitative understanding of thermodynamic interactions between the ice, ocean, and atmosphere in the vicinity of the ice edge and to determine how the state (concentration, thickness, floe size distribution) of the ice cover affects the relative importance of the ocean and atmosphere in these interactions.

While the direct effects of F_r on the surface and interior of an ice floe are well understood and fairly easy to treat in models, the input of F_r to the upper ocean and subsequent interaction with the ice cover have received surprisingly little attention. Yet it seems clear from a variety of evidence that solar heating of the water can have a major effect on the state of the ice cover. In the central Arctic, for example, *Maykut* [1982] utilized strain and heat balance data taken during the Arctic Ice Dynamics Joint Experiment (AIDJEX) to calculate time dependent changes in the area of open water (A_w) and in

Paper number 7C0229.
0148-0227/87/007C-0229$05.00

the total input of shortwave radiation to the ocean (Q_w) within a region spanning some 100–150 km. Over the course of the melt season he found that Q_w was roughly 50% as large as the energy used for melting at the upper surface of the ice. Because bottom ablation on multiyear floes in the region has been observed to be small, much of Q_w must have gone into lateral melting on floe edges. Observations at the main AIDJEX drifting station indicated about 10 m of lateral erosion during the summer (A. M. Hanson, personal communication, 1975), tending to support this view. If all of Q_w had gone into lateral melting, ice concentration in the region would have decreased by 8–10%. Although similar calculations cannot yet be carried out for the Antarctic ice pack, ice concentration there is believed to be substantially less than that in the Arctic and the importance of solar heating in the water correspondingly greater. Other studies [e.g., *Langleben*, 1972] have shown that the annual disappearance of the ice in many coastal regions can be explained only by the acceleration of decay processes resulting from solar heating of the water around the floes. The situation near the free boundaries of the pack is less certain, but heat input from the ocean can be large as weather systems transport the ice over warmer water or mesoscale circulations in the ocean (e.g., eddies) advect warmer water beneath the ice. Such effects, however, vary greatly in time and space, and the overall importance of oceanic heat transport relative to Q_w has yet to be established. Even in regions where the final stages of ice decay are dominated by the ocean, the thickness and concentration of ice reaching the MIZ will have been affected by upstream interactions with Q_w. It is evident that both large-scale and mesoscale models would benefit from more precise treatment of Q_w and the factors which affect its transport within the system.

Modeling the interaction of Q_w with the ice and ocean is complicated by ice movement, mechanical erosion, currents, meltwater stratification in the ocean, and a variety of other processes about which we have few details. An important step in developing a suitable model is to identify how Q_w is partitioned between lateral melting, bottom melting, temporary storage in the water, and loss to the atmosphere. Of particular interest is the horizontal energy transport at floe edges. By increasing A_w, lateral melting causes increased heat input to the water, setting up a positive feedback between Q_w, A_w and the net radiation balance of the ice-water mosaic. Previous studies have focused largely on the positive feedback aspects of the problem, neglecting much of the physics involved. In this regard, it should be noted that there is a strong coupling between dynamic and thermodynamic processes acting within the system. Divergence in the ice velocity field can produce large and rapid changes in A_w which may overwhelm changes produced by the thermodynamics. While this will impact the magnitude of Q_w and the importance of the positive feedback process, it should not significantly alter the thermal processes associated with Q_w.

To obtain a more quantitative understanding of how solar radiation affects the ice-ocean system, we have formulated simple, yet fairly realistic, heat balance models of the three most important system components: ice, leads, and the underlying water column. Results from the models provide information on the relative importance of ice thickness, lead width, floe perimeter, meteorological conditions, oceanic heat flux, and horizontal heat transfer rates at the ice-water interface. Predictions are compared with those of simpler models and applications to large-scale and mesoscale models discussed.

PREVIOUS WORK

The potential for lateral melting on floe edges to accelerate the disintegration of a sea ice cover was first recognized by *Zubov* [1945], who derived a simple equation to describe the process. He assumed that all the solar energy absorbed in a lead was immediately and completely used in lateral melting and that any change in ice thickness was negligible, i.e.,

$$Q_w\,dt = A_w(1-\alpha_w)F_r\,dt = \rho_i L_f H\,dA_w \tag{1}$$

where $\alpha_w = 0.1$ is the albedo of the water, $\rho_i = 900$ kg m^{-3} is the density of the ice, $L_f = 0.335$ MJ kg^{-1} is the latent heat of fusion of the ice, H is the ice thickness, and t is time. If we let $\xi_w = (1-\alpha_w)F_r/\rho_i L_f$, then the solution to (1) can be written

$$A_w = A_{w0}e^{\xi_w t/H} \tag{2}$$

where A_{w0} is the area of open water at time $t = 0$.

Doronin and Kheisin [1975] have pointed out that the simple exponential increase in A_w with time predicted by (2) is not likely to be realistic unless the fraction of open water is small. They argue that an increasing A_w/A_{w0} would eventually result in lead temperatures above the freezing point and in a greater proportion on the absorbed radiation being utilized for warming of deeper layers in the ocean. These effects would tend to slow down the actual increase in A_w. However, when *Langleben* [1972] attempted to apply the Zubov approach to the decay of ice in sheltered bays and fjords along the Canadian archipelago, he found that the decay rates obtained with (2) were too slow to explain the observed disappearance of the seasonal ice cover. To obtain a more realistic description of the decay process in these regions, Langleben modified the Zubov equation to take into account thinning of the ice. He assumed that any decrease in thickness was the result of melting at the upper surface, the amount being determined by the magnitude of the net shortwave radiation flux, i.e.,

$$A_i(1-\alpha_i)F_r\,dt = -\rho_i L_f A_i\,dH \tag{3}$$

where α_i is the albedo of the ice and A_i is the total area covered by ice. Integration of (3) gives the change of thickness with time,

$$H = H_0 - \xi_i t \tag{4}$$

where H_0 is the ice thickness at time $t = 0$ and $\xi_i = (1-\alpha_i)F_r/\rho_i L_f$. Substituting (4) into (1) and solving yields

$$A_w = A_{w0}\left(1 - \frac{\xi_i t}{H}\right)^{-\mu} \tag{5}$$

where $\mu = \xi_w/\xi_i = (1-\alpha_w)/(1-\alpha_i)$. With nominal values of α_i, α_w, and F_r, Langleben found that (5) predicted the disappearance of the ice in roughly half the time required by (2), in general agreement with his observations.

While the analytical solution obtained by Langleben appears to be more realistic than that of Zubov, it also neglects some important physics. In particular, it retains the assumption that all the energy absorbed by the water goes to lateral melting, the result of which is likely to be an artificially magnified rate of increase in A_w. In reality, a considerable amount of energy can be absorbed beneath the bottom of the ice where it would contribute to warming of the water and melting on the underside of the ice. The model described below explicitly treats these and other factors which affect heat transfer between the water and the ice.

THE LEAD MODEL

Approach to the Problem

As the first step in a more complete treatment of the problem, we will examine heat transfer and mass changes in a single lead under steady state conditions. We will then combine these results with equations describing ablation at the top and bottom of the surrounding ice to predict time dependent changes in ice concentration and thickness. Let us now consider a lead of width W and length L, bounded by ice of thickness H. Since L is typically much greater than W, we will represent the lead as a two-dimensional feature and consider only changes in width and depth. To simplify the problem further, we will assume that the water in the lead can be characterized by a single temperature, T_w. This assumption is supported by field measurements from Mould Bay, Prince Patrick Island, Northwest Territories (NWT) [*Perovich*, 1983] and from the Greenland Sea [*Maykut and Perovich*, 1985] which indicate that horizontal and vertical temperature gradients in leads are generally small. The heat balance equation for the lead can thus be written

$$W[(1-\alpha_w)F_r - I_w + F_L - \varepsilon_w\sigma T_w^4 + F_{sw} + F_{ew} + F_{wl}] - \rho_i L_f H(dW/dt) = \rho_w c_w HW(dT_w/dt) \quad (6)$$

where I_w is amount of shortwave radiation absorbed below the bottom of the ice, F_L is the incoming long-wave radiation, F_{sw} is the sensible heat flux, F_{ew} is the latent heat flux, F_{wl} is the flux of heat between the lead and the underlying ocean, ε_w is the long-wave emissivity of the water, $\sigma = 5.67 \times 10^{-8}$ W m^{-2} °K^{-4} is the Stefan-Boltzman constant, $\rho_w = 1000$ kg m^{-3} is the density of the water, and $c_w = 4185$ J kg^{-1} °K^{-1} is the specific heat of water. The sign convention is that heat fluxes into the lead are positive and out of the lead are negative. A schematic illustration of this situation is shown in Figure 1.

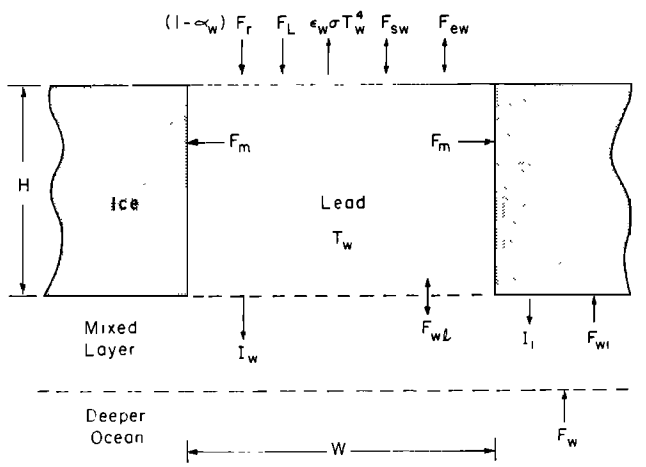

Fig. 1. Schematic illustration of energy fluxes in the lead and underlying water, where T_w is lead temperature, F_r is the incoming shortwave radiation, F_L is the incoming long-wave radiation, $\varepsilon\sigma T_w^4$ is long-wave radiation emitted from the surface of the lead, F_{sw} is the sensible heat flux, F_{ew} is the latent heat flux, F_m is the average horizontal heat flux at the lead wall, I_w is the amount of shortwave radiation transmitted through the lead and absorbed below the bottom of the surrounding ice, F_{wl} is the flux of heat associated with water exchange between the lead and underlying ocean, I_1 is the flux of shortwave radiation transmitted through the ice to the ocean, F_{wi} is the oceanic heat flux to the bottom of the ice, and F_w represents heat exchange with the deeper ocean.

Calculation of Fluxes

Net shortwave input at the surface of the lead is $W(1-\alpha_w)F_r$; however, part of this energy (WI_w) is absorbed below the ice and does not immediately contribute to the heat balance of the lead. This is because relative motion between the ice and water tends to advect I_w beneath the ice where it mixes with the surrounding water and contributes to the oceanic heat flux at the underside of the ice (F_{wi}). If $i_w(H)$ is defined as the fraction of the net shortwave radiation which is transmitted through a water layer of thickness H, then $I_w = i_w(1-\alpha_w)F_r$ and the amount of solar energy retained in the lead is $W(1-\alpha_w)(1-i_w)F_r$. The magnitude of i_w depends on the absorptive properties of the water, on the spectral distribution of F_r (i.e., on cloudiness), and on the thickness of the ice. To obtain a simple expression for $(1-\alpha_w)(1-i_w)$, the Bouguer-Lambert law was used to calculate i_w as a function of wavelength and water depth using spectral extinction coefficients for very clear water [*Tyler and Smith*, 1970; *Grenfell*, 1979] and incident spectra for both clear and cloudy skies [*Sauberer and Dirmhirn*, 1958; *Gast*, 1960]. The results were combined with spectral albedo data for Arctic water, then integrated over wavelength to find values for $(1-\alpha_w)(1-i_w)$ as a function of water depth under both clear and cloudy skies (Figure 2). The integrated results can be approximated by

$$(1-\alpha_w)(1-i_w) = a_1 + a_2 \ln(H) \quad (7)$$

where H is in meters; $a_1 = 0.5676$, $a_2 = 0.1046$ for clear skies; and $a_1 = 0.3938$, $a_2 = 0.1208$ for cloudy skies. In both cases the fit is quite good with correlation coefficients greater than 0.995.

Although incoming longwave radiation depends on the vertical distribution of atmospheric water vapor and temperature, a large part of F_L is emitted by clouds and water vapor close to the ground and can be approximated fairly well from surface observations. Several parameterizations of F_L under polar conditions have been suggested [*Marshunova*, 1966; *Idso and Jackson*, 1969; *Maykut and Church*, 1973]. For the calculations reported here, we have selected the relationship given by *Maykut and Church* [1973]

$$F_L = (0.7855 + 0.2232C^{2.75})\sigma T_a^4 \quad (8)$$

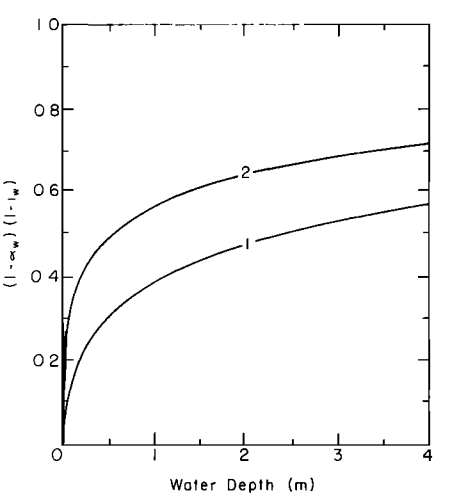

Fig. 2. Fraction of the incident shortwave radiation absorbed by Arctic water as a function of depth under cloudy (curve 1) and clear (curve 2) skies.

where C is the fractional cloud cover (0–1) and T_a is the air temperature at screen height. Values predicted by (8) appear to be accurate to within 7% under overcast skies and 12% under clear skies.

The sensible heat flux is given by

$$F_{sw} = \rho_a c_p C_s u(T_a - T_w) = K_s u(T_a - T_w) \quad (9)$$

where $\rho_a = 1.3$ kg m^{-3} is the density of the air, $c_p = 1004$ J kg^{-1} °C^{-1} is the specific heat at constant pressure, $C_s = 1.75 \times 10^{-3}$ is the bulk transfer coefficient for sensible heat, u is the wind speed, and $K_s = \rho_a c_p C_s$. The latent heat flux can be written, $F_{ew} = \rho_a L_v C_e u(q_a - q_{0w})$, where $L_v = 2.49$ MJ kg^{-1} is the latent heat of vaporization, $C_e = 1.75 \times 10^{-3}$ is the bulk transfer coefficient for latent heat, and q_a and q_{0w} are specific humidities in the air and at the surface of the lead. For our calculations we will express F_{ew} in terms of saturation vapor pressure e_s and relative humidity r

$$F_{ew} = K_e u(re_{sa} - e_{sw}) \quad (10)$$

where air at the surface is assumed to be at saturation, $K_e = 0.622\rho_a L_v C_e/p_0$ and $p_0 = 1013$ mbar is the atmospheric pressure at the surface. To calculate saturation vapor pressures, we will use the unwieldy, but computationally convenient, form suggested by *Maykut* [1978]

$$e_s = b_1 T^4 + b_2 T^3 + b_3 T^2 + b_4 T + b_5 \quad (11)$$

where $b_1 = 2.7798202 \times 10^{-6}$, $b_2 = -2.6913395 \times 10^{-3}$, $b_3 = 0.97920849$, $b_4 = -158.63779$, and $b_5 = 9653.1925$.

Heat exchange between the lead and the underlying ocean (F_{wl}) can occur as a result of vertical temperature gradients in the water or because of mechanical mixing associated with movement of the ice and water. Unfortunately, there is little information available concerning the magnitude or even the direction of F_{wl}, and for the present, it is assumed to be negligible in comparison to other components of the energy balance equation.

Crucial to the performance of the model is an appropriate description of lateral melting on the lead walls. One approach is to assume that energy transport to the ice edge is so rapid that T_w remains at the freezing point; i.e., all available energy goes to lateral melting. This is analogous to the Zubov-Langleben treatment (except that I_w does not contribute directly to dW/dt) and will be referred to as the instantaneous heat transfer (IHT) case. Since T_w is known, (6) can, for given thermal forcing, be solved immediately for dW/dt. One consequence of this assumption is a linear increase in lateral melt rate with increasing W. This result, however, is contrary to intuition. As the lead widens, it becomes increasingly unlikely that all the absorbed heat can be transported to the ice walls. In fact, water temperatures as high as +10°C have been observed in the middle of large polynyas [*Bulgatov and Zakharov*, 1978]. More reasonable would be an increase in T_w with W which would produce a corresponding increase in the amount of heat lost to the atmosphere and a less rapid increase in dW/dt than predicted by the IHT assumption.

Laboratory observations [*Josberger*, 1979; *Josberger and Martin*, 1981] of ice melting in salt water revealed the presence of a complex boundary layer adjacent to vertical ice walls. The rate at which heat can be transported to the wall is regulated by the properties of this boundary layer. Depending on the salinity and far field temperature of the water, convective motions in the boundary layer were found to be turbulent, laminar, or bidirectional laminar, with more than one flow regime frequently existing along a single wall. Lateral melt rates were generally greatest on the part of the wall adjacent to the turbulent flow regime. For turbulent flow, *Josberger* [1979] found that the vertically averaged lateral melt rate M_r could be parameterized by

$$M_r = m_1 \Delta T_w^{m_2} = 0.5(dW/dt) \quad (12)$$

where $\Delta T_w = T_w - T_f$ is the elevation of the water temperature above the freezing point, T_f is the salinity determined freezing point temperature, $m_1 = 2.85 \times 10^{-7}$ m s^{-1} °C$^{-1.36}$ and $m_2 = 1.36$. Simultaneous solution of (6) and (12) then yields T_w and M_r (or dW/dt). This method will subsequently be referred to as the boundary layer parameterization, or BLP.

The applicability of (12) to actual field conditions was examined by *Perovich* [1983] using data from a single static lead near the coast of Prince Patrick Island, NWT. It was found that (12) consistently underestimated M_r and, over a 3-week period, predicted only one-third the observed melting. The best fit to the observations was obtained with $m_1 = 16 \times 10^{-7}$ m s^{-1} °C$^{-1.36}$, more than 5 times the average value measured in the laboratory. While the nearshore observations are not necessarily typical of conditions elsewhere in the Arctic basin, they suggest that currents, wind mixing, or other processes in natural leads can affect the structure of the boundary layer and accelerate the horizontal heat transport at floe edges. Whether transport rates in dynamically active parts of the ice pack would be even greater is not yet clear.

Results for a Single Lead

The lead model described above includes much of the physics neglected in previous treatments. In particular, it allows heat buildup in the lead, exchange of energy with the atmosphere and underlying ocean, and inclusion of the boundary layer adjacent to the lead walls. The model also provides a framework which could, in principle, accommodate parameterizations of mechanical erosion and heat exchange between the lead and underlying ocean. In this section we will investigate the steady state response of the model to differences in W, H, thermal forcing, and assumptions regarding the rate of horizontal heat transport. The model will be applied to perennial ice in the central Arctic and to first-year ice in the nearshore region under typical midsummer conditions. Model response in each region will be examined for the IHT case, the laboratory BLP case, and the field BLP case.

Combining equations (6)–(12), we can rewrite the governing equation

$$\begin{aligned}&[a_1 + a_2 \ln (H)]F_r - \varepsilon_w \sigma T_w^4 + (0.7855 + 0.2232C^{2.75})\sigma T_a^4 \\ &+ K_s u(T_a - T_w) + K_e u[b_1(rT_a^4 - T_w^4) + b_2(rT_a^3 - T_w^3) \\ &+ b_3(rT_a^2 - T_w^2) + b_4(rT_a - T_w) + b_5(r - 1)] \\ &- \rho_i L_f H\left(\frac{1}{W}\frac{dW}{dt}\right) = 0 \end{aligned} \quad (13)$$

where $dT_w/dt = 0$ and F_{wl} is assumed to be negligible. To determine dW/dt for a particular W in the IHT case, we must specify H, F_r, T_a, u, r, and C. For the BLP cases where (12) is used to replace dW/dt with a function of ΔT_w, far field salinity in the lead (S_w) must also be known in order to calculate T_f. The result is then a fourth-order polynomial in T_w which is solved using the Newton-Raphson iterative method [*Horn-*

TABLE 1. Summary of Environmental Conditions Used in the Central Arctic and Nearshore Calculations

Parameter	Central Arctic	Near-shore
F_r, W m^{-2}	242	291
T_a, °C	0	2
H, m	3	2
u, m s^{-1}	5	5
C	0.9	0.9
S_w, ‰	30	3
T_f, °C	−1.62	−0.16
α_i(H > 0.75 m)	0.5	0.3
i_0(H > 0.75 m)	0.35	0.63

beck, 1975]. Knowing T_w, M_r is calculated from (12). Assumed environmental conditions (Table 1) in the near shore region were derived from the observations of *Langleben* [1966] and *Perovich* [1983], while those in the central Arctic were taken from *Maykut* [1982].

The predicted dependence of M_r on W for the two regions is shown in Table 2 and Figures 3*a* and 3*b*. As with the

TABLE 2. Influence of Lead Width and Boundary Layer Parameterization on Melt Rates (Meters per Day) and Energy Fluxes (Watts per Square Meter) under Central Arctic and Nearshore Conditions

Case	W, m	M_r	ΔT_w	F_{sw}	F_{ew}	Net LW	F_{mw}
			Nearshore				
Lab	1	0.01	0.41	18	6	−20	−142
	5	0.04	1.38	7	−2	−25	−118
	10	0.07	2.08	−1	−9	−28	−100
	50	0.17	4.02	−23	−31	−37	−47
	100	0.21	4.67	−31	−38	−41	−28
	500	0.25	5.43	−39	−47	−45	−7
	1,000	0.26	5.55	−41	−49	−45	−3
	5,000	0.27	5.65	−42	−49	−46	−1
	10,000	0.27	5.66	−42	−50	−46	0
Field	1	0.01	0.40	22	10	−18	−152
	5	0.05	0.37	18	7	−19	−144
	10	0.10	0.66	15	4	−21	−136
	50	0.37	1.95	1	−8	−27	−104
	100	0.58	2.77	−9	−16	−31	−82
	500	1.13	4.58	−30	−37	−40	−31
	1,000	1.29	5.05	−35	−43	−43	−17
	5,000	1.46	5.53	−40	−49	−45	−4
	10,000	1.48	5.60	−41	−50	−45	−2
			Central Arctic				
Lab	1	0.01	−1.21	14	2	−21	−123
	5	0.03	−0.53	6	−3	−24	−107
	10	0.05	−0.01	0	−7	−27	−94
	50	0.12	1.68	−19	−23	−35	−51
	100	0.16	2.37	−27	−30	−38	−33
	500	0.21	3.27	−37	−40	−42	−9
	1,000	0.22	3.42	−39	−41	−43	−5
	5,000	0.23	3.56	−41	−42	−44	−1
	10,000	0.23	3.57	−41	−43	−44	0
Field	1	0.01	−1.46	17	5	−19	−131
	5	0.03	−1.24	15	3	−20	−126
	10	0.06	−1.04	13	1	−21	−121
	50	0.23	−0.11	1	−6	−25	−98
	100	0.38	0.55	−6	−12	−29	−81
	500	0.86	2.26	−26	−29	−37	−36
	1,000	1.03	2.80	−32	−34	−40	−22
	5,000	1.22	3.40	−39	−41	−43	−5
	10,000	1.25	3.50	−40	−42	−44	−2

The shortwave radiation deposited in the lead is 138 W m^{-2} in the near shore case and 128 W m^{-2} in the central Arctic case.

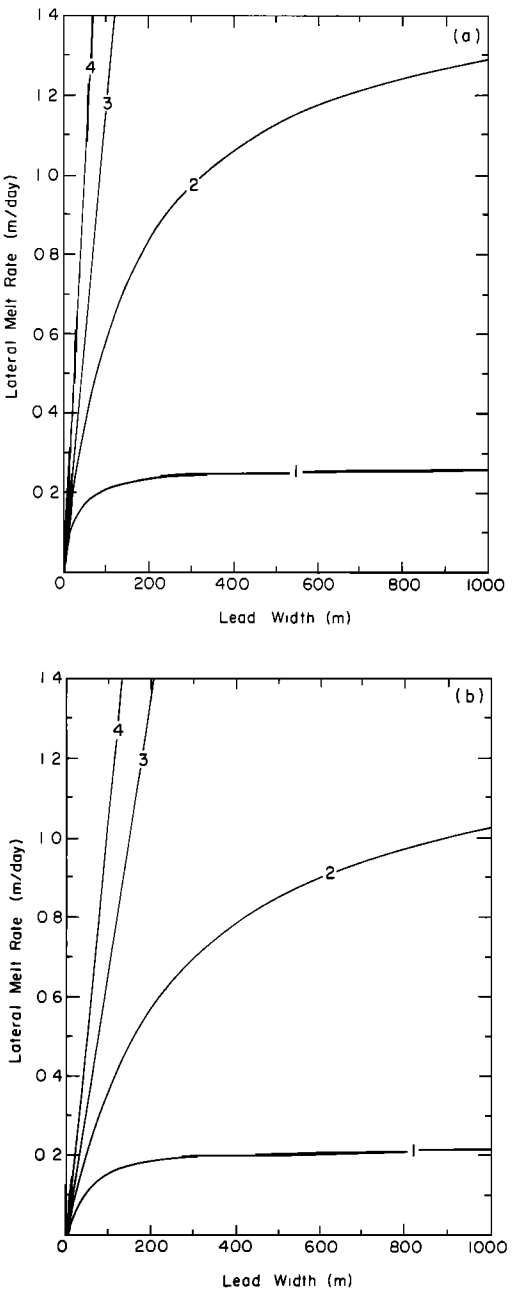

Fig. 3. Comparison of steady state lateral melt rates predicted by the laboratory BLP (curve 1), the field BLP (curve 2), the IHT assumption (curve 3), and the Zubov-Langleben formulation (curve 4) under (*a*) nearshore and (*b*) central Arctic conditions.

Zubov-Langleben (Z-L) formulations, melt rates in the IHT case increase linearly with lead width (i.e., M_r/W is a constant), but at a somewhat slower rate. Differences between IHT and Z-L values are less than might be expected strictly on the basis of I_w because the sum of the turbulent and longwave fluxes augment solar heat input to the lead by about 15% in both regions. In the nearshore region, the ratio of the Z-L melt rate to that of the IHT is about 1.72, while the central Arctic ratio is 1.56, the decrease being due largely to the reduction in I_w because of greater ice thickness. The IHT case predicts that dW/dt in the nearshore region would increase from about 2.3 cm d^{-1} in a 1-m lead to 23 m d^{-1} in a 1-km polynya. A similar increase was also found in the central

Arctic. The weakness of the IHT and Z-L formulations becomes evident with the increasingly unrealistic melt rates at large values of W.

Inclusion of a boundary layer parameterization leads to greatly reduced melt rates in the wider leads, particularly in the case of the laboratory BLP where M_r is relatively insensitive to values of $W > 100$ m. The variation of M_r with W in the field BLP case is close to that of the IHT when $W < 50$ m, but the difference increases sharply with W above 50 m. Significant increases in M_r continue until W reaches the 1- to 2-km range. This behavior is a direct result of the dependence of M_r on T_w in (12). For the melt rate to increase, T_w must rise, leading to greater long-wave and turbulent heat losses to the atmosphere. Unlike the IHT case, values of T_w are usually greater than T_a in the BLP cases, so that the turbulent fluxes result in a net heat loss instead of a gain. In the central Arctic case, for example, the laboratory BLP predicts that the heat lost to the atmosphere over a 100-m lead would be a factor of 20 larger than that over a 1-m lead (Table 2). However, between 100 m and 1 km the increase is only about 30%. This is because T_w asymptotically approaches a limiting value (T_{lim}) where increased solar absorption is balanced by greater atmospheric losses. While T_{lim} is essentially the same for both BLP cases (3.6°C for central Arctic conditions and 5.7°C for nearshore conditions), the rate of approach is considerably different. If we define the relaxation width W_r as the width at which $(T_w - T_f)$ reaches $(1 - e^{-1})(T_{\text{lim}} - T_f)$, we find for the central Arctic that W_r is 50 m with the laboratory BLP and 350 m with the field BLP; equivalent values in the nearshore region are 40 m and 300 m. The heat lost through lateral melting can be compared with other components of the energy balance if we multiply the horizontal heat flux to the wall ($F_m = -\rho_i L_f M_r$) by H and divide by the area of the lead surface, i.e., $F_{mw} = F_m H/W$. It can be seen from Table 2 that F_{mw} dominates the energy balance until W reaches 50–100 m in the laboratory BLP and several hundred meters in the field BLP. Above these values, F_{mw} decreases slowly in importance relative to F_s, F_e, and the net long wave.

BLP calculations were also carried out to determine the effect of ice thickness on lateral melt rates. As can be seen from Figure 4, the dependence of M_r on H and W is complex. An increase in H reduces I_w, allowing more solar heat to be retained by the lead. At the same time, however, thicker ice means that more energy is required to increase W by a given amount. When the lead is very narrow or the ice fairly thick, these two effects tend to balance, and M_r is nearly independent of H. In wider leads the I_w effect initially dominates the balance, and lateral melt rates in thin ice increase sharply with H. With continued increases in H the amount of heat lost at the wall becomes increasingly important until, at some point, the two effects reach an equilibrium. The thickness at which this occurs increases with W. Interestingly, there are situations where two different values of H will yield the same melt rate. This is a consequence of the dependence of I_w on H, as can be seen from (13). For a particular choice of M_r and W, (13) can be written in the form, $H + a \ln(H) + b = 0$, which can have a double-valued solution when H and W are small. Growth rate contours for the laboratory BLP have nearly the same pattern as that shown in Figure 4, except that the magnitudes are a factor of 4–5 less.

In general, the lateral melt rate increases as the net flux of heat through the surface of the lead becomes larger, i.e., when F_r and T_a increase or when u decreases. However, the magnitude of the change depends on the surface area (width) of the lead. An example of this dependence is shown in Figure 5, which gives M_r as a function of T_a and W. Although warmer air temperatures increase F_s, F_e, and F_L, the additional energy input in a narrow lead is small in relation to the amount used in lateral melting so that M_r is relatively insensitive to changes in T_a. Because the heat input to the lead is the product of W and the net flux, dM_r/dT_a increases fairly sharply as the lead widens. At the same time, increasing W causes T_w to rise, which reduces the rate at which the net flux increases. As we saw earlier, the eventual result is that an equilibrium flux balance is achieved for very wide leads and no further changes take place. Thus in the laboratory BLP the curves for 1 km and 10 km are nearly identical, while the field BLP curves continue to change until W reaches 2–3 km. The response of the lead to changes in F_r and u are similar to those for T_a.

It seems clear from these calculations that previous treatments have overestimated the positive feedback between F_r and A_w, not only as a result of assigning I_w to lateral melting but also by neglecting what can be substantial losses of heat to the atmosphere. While results from the BLP simulations conform to our intuition, it is by no means certain that either the

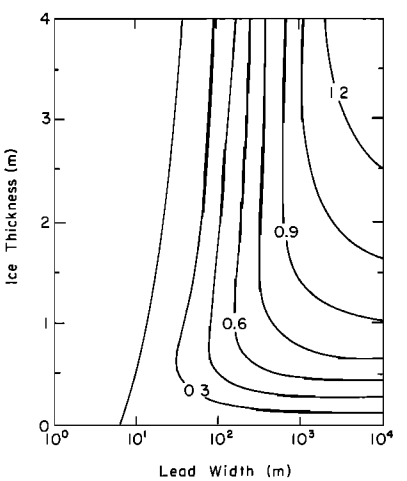

Fig. 4. Contours of lateral melt rate (in meters per day) as a function of lead width and ice thickness under central Arctic conditions using the field BLP.

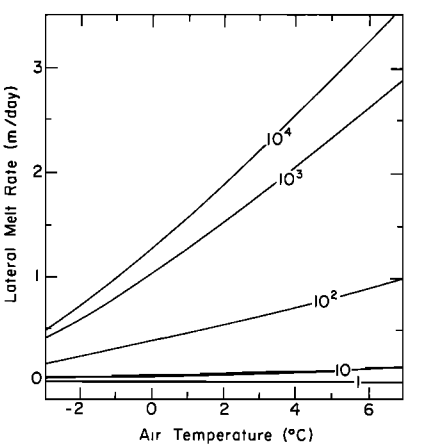

Fig. 5. Effects of air temperature on lateral melt rates for lead widths of between 1 m and 10 km using the field BLP and central Arctic conditions.

Mould Bay or laboratory parameterizations are representative of heat transport rates in a mobile ice pack. We see, however, that the greater the magnitude of m_1 in (11), the larger W_r becomes, and the closer the BLP results approximate those of the IHT when $W < W_r$. Paradoxically, the fact that M_r tends to become less dependent on W as the leads widen means that some assumption regarding the distribution of lead widths will need to be made in regional calculations if a significant fraction of A_w is made up of wider leads. This is an undesirable complication in any attempt to formulate a more realistic, yet relatively simple, larger-scale model and will be discussed in more detail below.

REGIONAL ICE DECAY

To this point we have not considered melting on the horizontal boundaries of the ice and have ignored possible effects of I_w on the oceanic heat flux. In this section we look at the behavior of a region containing an idealized system of leads and floes. Leads are assumed to be equally spaced and of equal width. The system is allowed to evolve through time, taking into account warming of the water, thinning of the ice, and changing ice concentration.

Treatment of Mass Changes

The energy balance equation at the surface of melting ice is

$$(1 - \alpha_i)(1 - i_0)F_r + F_L - \varepsilon_i \sigma T_0^4 + F_{si} + F_{ei} + F_c = -\rho_i L_f (dH/dt)_0 \quad (14)$$

where $T_0 = 273°K$ is the surface temperature of the ice, F_c is the conductive heat flux in the ice, and i_0 is the fraction of the net shortwave radiation that does not contribute directly to surface melting. The long-wave and turbulent fluxes over the ice are computed using (8)–(10) with T_0 substituted for T_w. Temperature gradients are small in melting ice and F_c is assumed to be negligible. Melting at the surface of snow-covered ice can also be calculated with (14) if a_i, i_0, and ρ_i are replaced with values appropriate for snow.

Because ice is a translucent material, only part of the net shortwave radiation is immediately available for melting at the surface, the remainder being distributed between latent heat storage in the interior of the ice and transmission to the underlying water. Each of these energy sinks was treated separately in the model. Following the arguments of *Grenfell and Maykut* [1977], the ice was assumed to consist of two regions: (1) a surface layer, of the order of 10 cm in thickness, where absorbed radiation goes entirely to surface melting, and (2) a lower layer where light attenuation is closely approximated by Beer's law. Energy absorption in the upper layer is complicated by large vertical changes in the spectral distribution of the penetrating radiation which cannot be described without a detailed radiative transfer model. To avoid this complication, we parameterized absorption in the surface layer by $(1 - i_0)(1 - \alpha_i)F_r$. The magnitude of i_0 depends on the type of ice and the spectral distribution of F_r. *Grenfell and Maykut* [1977] calculate that i_0 for melting white ice is 0.35 when overcast and 0.18 when clear; for blue ice it is 0.63 when overcast and 0.43 when clear. In the central Arctic calculations we selected $i_0 = 0.35$ and $\alpha_i = 0.5$, while in the nearshore calculations we used 0.63 and 0.3. When $H < 75$ cm, both i_0 and α_i become dependent on H [*Grenfell*, 1979]. In this situation we used the approximations given by *Perovich* [1983].

The amount of solar energy transmitted through the surface layer is $i_0(1 - \alpha_i)F_r$, while the amount transmitted to the ocean (I_i), assuming Beer's law attenuation, is

$$I_i = i_0(1 - \alpha_i)F_r e^{-\kappa(H - H_0)} \quad (15)$$

where $\kappa = 1.5\ m^{-1}$ is the bulk extinction coefficient in the ice and $H_0 = 0.1$ m is the thickness of the surface layer. Shortwave radiation absorbed in the lower layer of the ice goes largely to internal melting rather than to direct changes in thickness. This increases the brine volume in the ice and decreases the amount of energy needed for subsequent mass changes at the boundaries. The energy absorbed in the lower layer is taken into account by altering the magnitude of the latent heat of fusion. Assuming that this energy is used entirely for internal melting and that the change in brine volume is uniform throughout the slab, the change in L_f is

$$dL_f/dt = i_0(1 - \alpha_i)[1 - e^{-\kappa(H - H_0)}]F_r/\rho_i H \quad (16)$$

The primary reason for allowing L_f to decrease during the melt progression is that this provides a much more realistic description of time-dependent changes in dH/dt than do methods which assign all available energy to surface melting. The net result is an ice cover which initially thins more slowly but which melts more rapidly during the final decay phase when the brine volume is large. In perennial ice this approach also yields a much better estimate of H at the onset of freezing.

The flux balance at the underside of the ice is

$$\rho_i L_f (dH/dt)_H = F_c - F_{wi} \quad (17)$$

As before, F_c is assumed to be negligible. The problem is how to determine F_{wi}. We will assume that energy input at the bottom of the ice is proportional to the total amount of energy present in the underlying water (E_w) and to the ice concentration (G_0), i.e.,

$$F_{wi} = RE_w/G_0 = -\rho_i L_f (dH/dt)_H \quad (18)$$

where R is the rate of energy loss from the underlying water. The change in E_w with time is given by

$$dE_w/dt = G_0 I_i + (1 - G_0)(I_w + F_{wl}) - G_0 F_{wi} + F_w \quad (19)$$

where F_w is the heat exchanged with deeper layers of the ocean. Assuming that F_{wl} and F_w are negligible, then combining (7), (15), and (18) with (19), we obtain

$$dE_w/dt = [G_0 f_1 + (1 - G_0)f_2]F_r - RE_w \quad (20)$$

where $f_1 = i_0(1 - \alpha_i)e^{-\kappa(H - H_0)}$ and $f_2 = 1 - \alpha_w - a_1 - a_2 \ln(H)$. For given thermal forcing, (6), (12), (14), (16), (18), and (20) define the behavior of the ice and water system. The first step in the solution of the system was to solve (6) for dT_w/dt. A new ΔT_w was then determined and substituted into (12) to calculate the amount of lateral melting. Because of the assumed geometry, it was then possible to relate M_r directly to dG_0/dt. The amount of top and bottom melting was found from (14) and (18), and the thickness was adjusted. Finally, new values of E_w and L_f were computed and the whole procedure repeated. A time step of one twentieth of a day was used in the calculations.

Oceanic Heat Flux at the Underside of the Ice

We will now look more carefully at the heat flux to the bottom of the ice and try to choose a suitable value for R. If

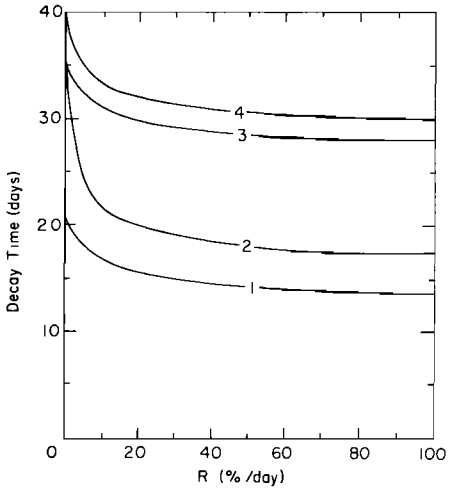

Fig. 6. Decay time of an idealized ice cover with 10-m leads as a function of initial ice concentration and the rate of energy loss from the underlying water (R). Under nearshore conditions, calculations of t_d were carried out with $G_0 = 0.5$ for the IHT (curve 1) and laboratory BLP (curve 2); corresponding values with $G_0 = 0.9$ are shown in Curves 3 and 4.

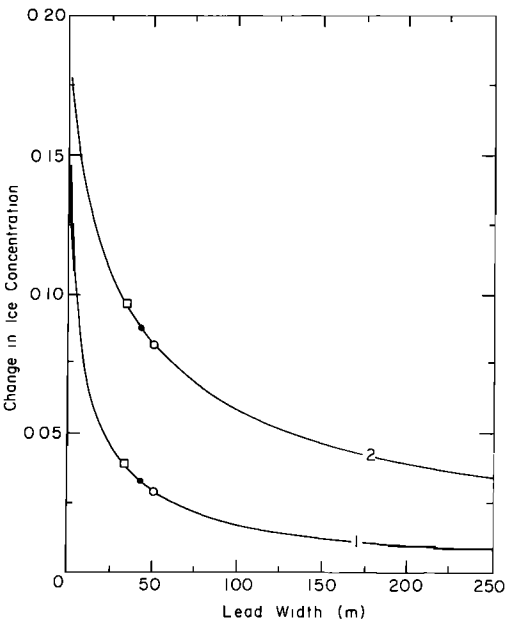

Fig. 7. Change in ice concentration over a 60-day period as a function of lead width using central Arctic conditions and an initial concentration of 0.9. Results using the laboratory BLP are shown in curve 1 and those of the field BLP in curve 2. Corresponding results for selected two dimensional geometries are indicated by symbols: a 4 :1 rectangular lead by an open box, a square lead by a solid circle, and a circular lead by an open circle.

the rate of shortwave input beneath the ice is constant and the initial energy content of the underlying water is zero, (20) can be integrated to obtain

$$E_w(t) = [G_0 f_1 + (1 - G_0) f_2] F_r (1 - e^{-Rt})/R \qquad (21)$$

and from (18)

$$F_{wi} = [G_0 f_1 + (1 - G_0) f_2] F_r (1 - e^{-Rt})/G_0 \qquad (22)$$

Regardless of the value of R, F_{wi} asymptotically approaches an equilibrium where it equals the rate of energy input. The time it takes to reach equilibrium is inversely proportional to R, suggesting that the choice of R may not be critical to model results after the first few days.

The general applicability of the above solution is of course limited, since in nature the energy input will be continually varying in response to changes in H, G_0, and F_r. To obtain a more precise picture of how the choice of R affects F_{wi}, the complete set of equations was integrated, and F_{wi} was plotted as a function of time for different values of R. The results indicated that F_{wi} is relatively insensitive to R unless it is less than about 10–20% per day. The influence of R on the time taken for complete decay of the ice cover (t_d) is shown in Figure 6. In all cases, t_d was also only sensitive to R when values were less than about 10% per day. While the precise value of R remains uncertain, one would expect it to be greater than 10% per day. Somewhat arbitrarily, a value for R of 50% per day was chosen for use in subsequent calculations. Any errors associated with this choice of R should be small.

Time-Dependent Results

Initial attention was focused on the relationship between dG_0/dt and lead size. Model runs were made under nearshore and central Arctic conditions using both boundary layer parameterizations and a variety of lead widths. While ice in the nearshore region invariably vanished in a month or less, concentration changes in the central Arctic were relatively slow and could be followed over a longer period of time. The change in G_0 over a 60-day period is graphed in Figure 7 as a function of initial lead width, assuming an initial concentration of 0.9. As expected, dG_0/dt was greatest when the leads were narrow and diminished quickly for wider leads. The reason for this is that in spite of smaller lateral melt rates, narrower leads utilize a greater fraction of the absorbed shortwave energy for lateral melting. The net result is that an ensemble of smaller leads will produce a greater change in G_0 than will an equal area of larger leads. Physically, this means that the more broken up the ice pack, the greater the efficiency of the heat transport to floe edges. Except in the case of very narrow leads, dG_0/dt for the field BLP was roughly twice as large as it was for the laboratory BLP. With the IHT assumption, the change in G_0 was 0.24, substantially larger than any of the values obtained using the BLPs.

Even in cases where the different treatments predict similar total decay times t_d, decay patterns can be strikingly different. This was particularly evident in the nearshore simulations (see Table 3) where, except for the Zubov treatment, total decay times were all within about 3 days of one another (Figure 8). The importance of taking into account changes in H is clear from the unrealistically large values of t_d predicted by Zubov. The primary difference between the other cases was in the relative importance of dH/dt and dG_0/dt. For the standard IHT and BLP cases the ice disappeared largely as a result of thinning, while in the case of Langleben the primary mechanism was lateral melting. Decay time for the standard IHT case was slightly less than that predicted by Langleben because more energy was added to the ice and leads as a result of the turbulent fluxes. Increased values of t_d in the BLP cases reflect both the heat losses to the atmosphere and the somewhat greater ice concentration. It is interesting to note that while the IHT and BLP treatments reduced the feedback between F_r and A_w, they introduced a strong positive feedback

TABLE 3. Summary of Regional Ice Decay for the Different Lead Formulations Assuming an Initial Ice Concentration of 0.9

Case	W, m	t_d, days	H, m	G_0	Total Ice Melt, % Lateral	Bottom	Top
			Nearshore				
Zubov		61.4	2.00	0.00	100	0	0
Langleben		28.0	0.37	0.00	32	0	68
IHT		27.6	0.00	0.11	24	28	48
IHT*		28.4	0.39	0.00	31	21	48
Lab BLP	1	29.6	0.00	0.72	12	31	57
	10	30.5	0.00	0.84	5	32	63
	100	31.1	0.00	0.89	1	33	66
Field BLP	1	29.1	0.00	0.60	15	31	54
	10	29.9	0.00	0.76	11	31	58
	100	30.7	0.00	0.86	4	32	64
			Central Arctic				
Zubov		110.5	3.00	0.00	100	0	0
Langleben		60.7	0.89	0.00	43	0	57
IHT		···	1.62	0.71	27	24	49
IHT*		···	1.70	0.66	33	20	47
Lab BLP	1	···	1.66	0.75	23	24	53
	10	···	1.75	0.83	14	24	62
	100	···	1.82	0.88	4	23	73
Field BLP	1	···	1.63	0.72	26	24	50
	10	···	1.68	0.76	22	24	54
	100	···	1.77	0.84	12	24	65

In cases where complete decay was not achieved, reported values are those obtained after 60 days of integration.

*Includes heat exchange between lead and underlying water.

between I_w and $(dH/dt)_H$ which also proved to be effective in removing the ice. In the IHT case it can be argued that mass exchange between the lead and the underlying water would result in a net input of heat to the lead. To examine what would happen in this situation, we considered an alternate IHT case (denoted by IHT* in Table 3) in which F_{wl} was assumed to be proportional to lead area and E_w, analogous to the treatment of F_{wi}. The relatively small changes in $(dH/dt)_H$ and dG_0/dt were sufficient to cause the ice to vanish by lateral ablation rather than thinning, demonstrating that F_{wl} can be an important factor in determining decay patterns, particularly in areas of seasonal ice.

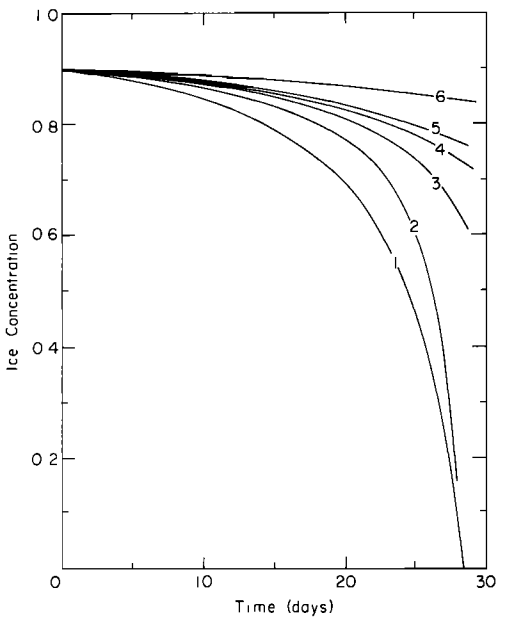

Fig. 8. Change in ice concentration under nearshore conditions as a function of time for various lead formulations: curve 1, Langleben; curve 2, IHT; curve 3, field BLP with 1-m leads; curve 4, laboratory BLP with 1-m leads; curve 5, field BLP with 10-m leads; and curve 6, laboratory BLP with 10-m leads.

The central Arctic BLP simulations resulted in a 40–45% reduction in H and relatively small decreases in G_0 which were again dependent on lead size. The Langleben formulation predicted complete decay of the ice cover in only 60.7 days. This was in large part due to a neglect of long-wave radiation losses which caused surface ablation to be seriously overestimated and an unrealistic acceleration of the feedback between F_r and A_w. The Langleben equation did fairly well in the nearshore region because the long-wave losses were nearly balanced by gains from the turbulent heat fluxes, but this will not usually be the case in most parts of the polar ice pack.

Application to Other Geometries

The above treatment can easily be extended to leads with more complex geometries. The governing equation for a lead with finite horizontal dimensions is

$$A_w[(1-\alpha_w)(1-i_w)F_r + F_L - \varepsilon_w\sigma T_w^4 + F_{sw} + F_{ew} + F_{wl}] - P_wH\rho_iL_fM_r = c_w\rho_wA_wH(dT_w/dt) \quad (23)$$

where P_w is the lead perimeter. Multiplying this equation by $2/P_w$ gives an equation which is identical to (6), except that W is replaced by the term $2A_w/P_w$. Thus in three dimensions the ratio of water area to lead perimeter is equivalent to lead width in the two-dimensional treatment and it is straightforward to extend the previous results to more realistic geometries using appropriate geometric formulas for area and perimeter. Figure 7 illustrates results obtained using equal areas of circular, square, and rectangular (4:1) leads. The rectangular lead, which had the smallest area to perimeter ratio, experienced the greatest change in ice concentration, while the circular lead with the largest ratio had the smallest change. Analogous to the two-dimensional case, the open water geometry that contains the greatest lead perimeter produces the greatest amount of lateral melting.

A serious drawback to the above calculations is that regular lead geometries do not begin to describe the complex distribution of open water within a real ice cover. Airborne imagery show that the size and shape of open water areas in the summer ice pack vary over a wide spectrum. Although the BLP formulation can, in principle, predict M_r for each particular lead size and shape, this is neither desirable nor feasible on a regional basis. Fortunately, it can be seen in Figure 3 that the $M_r(W)$ obtained from the field BLP is relatively linear up to widths of 100–200 m. Since the majority of leads usually do not exceed this size range, it should be possible to approximate $M_r(W)$ by a straight line under most conditions. Lacking specific information on spatial and temporal changes in floe size distribution, let us instead choose a characteristic lead size (W_c), say, the median width in the region. Solving (12) and (13), we obtain $M_r(W_c)$ which defines the slope of the $M_r(W)$ line. The result of assuming a linear dependence is that lateral melt rates will be slightly underestimated in leads narrower than W_c and overestimated in wider leads. If W_c has been chosen well, the errors will tend to cancel. This will of course not be the case if a substantial fraction of the area is occupied by very

large leads. A linear $M_r(W)$ is equivalent to saying that T_w is independent of lead size, i.e., the entire water matrix in the region can be characterized by a single temperature which depends on the choice of W_c. Knowing T_w, we can calculate the amount of energy used in lateral melting without needing to know anything further about the geometry or number of leads in the region. This is analogous to the IHT treatment, except that it takes into account the effect of lead warming on heat exchange with the atmosphere. If used in conjunction with imagery or models that provide information on variations in floe size distribution, W_c can be specified as a function of location and/or time. Although we have focused on lead width, open water areas could have been described equally well by a characteristic area to perimeter ratio.

MIZEX OBSERVATIONS

The above calculations indicate that accurate predictions of the interaction of F_r with the ice and upper ocean cannot generally be obtained with a simple Zubov or Langleben approach. The IHT formulation offers a much more realistic description of the system and can easily be accommodated in existing large-scale models; however, it too probably overestimates dG_0/dt, and it is likely that some form of the BLP will be needed in more detailed models. Unfortunately, previous experimental work on lateral melting has been largely confined to situations which are not typical of the ice pack as a whole. We have seen that large differences exist between horizontal heat transport rates in the laboratory and in a static lead, and it seems reasonable to ask whether similar differences might not exist between leads in static and dynamically active ice covers.

To address this question, lateral ablation and CTD measurements were carried out at the edge of a large, multiyear floe during the Marginal Ice Zone Experiment (MIZEX) in the Greenland Sea. Dynamic activity around this floe, located adjacent to the drifting ship *Polarqueen*, was high, and leads were often filled with brash derived from the breakup of nearby first-year floes. Because there appeared to be significant differences in the amount of open water and brash around the floe, periodic wall profiles and ice thickness data were taken at five different edge sites. Water salinity and temperature profiles were measured at one or more of these sites at 1- to 2-day intervals. In general, ablation rates were low during the first 3–4 weeks of the drift because most of the absorbed shortwave energy went almost immediately to the melting of brash. However, on day 191 (July 9) the floe entered warm water near the extreme edge of the pack which resulted in the disappearance of the brash and a dramatic increase in ablation rates. Lateral melting at site 1, for example, totaled about 0.8 m over the next 2 days, somewhat more than the total for the preceding three weeks (Figure 9). Rapid melting continued for the final week of the drift (days 193–200), but was complicated at some sites by mechanical erosion which totaled as much as 10 m.

Results of the lateral ablation measurements are summarized in Table 4. At most sites, melt rates were fairly constant with depth, suggesting that water in the leads was usually well mixed. This conclusion is supported by the conductivity-temperature-depth (CTD) measurements which showed salinity gradients of no more than 1–2‰ in the upper few meters, even during periods of strong melting. The ablation profile at site 4 is an exception and difficult to explain unless we assume

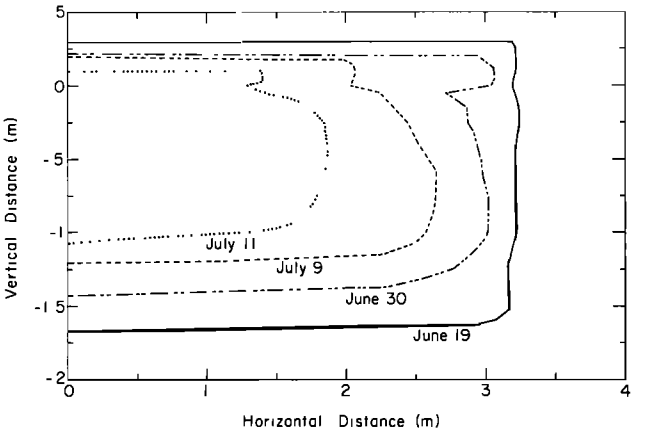

Fig. 9. Sequential wall profiles measured at site 1 during MIZEX '84.

that the water was stratified and that the primary heat source was solar radiation. CTD data were not taken at this site, and we have no evidence to indicate whether this was the case. The opposite pattern occurred at site 1 during the frontal crossing (days 191–193), and it is evident that heat was being entrained from the underlying water (i.e., $F_{wl} > 0$). Although processes and conditions in the MIZ are generally more complex than those elsewhere in the polar ocean, these results can still be used to compare average heat transfer rates with those observed in the static ice and in the laboratory. To facilitate this comparison, we again let $m_2 = 1.36$ and calculated values of m_1 from (12) during periods when there was no mechanical erosion. Results for each site are given in Table 4.

Calculated values of m_1 can be divided into two categories: (1) those for which concurrent CTD data were available at the site, and (2) those where salinity and temperature data from a different site had to be used. Results in the first category are fairly consistent and in good agreement with the Mould Bay value. Results in the second category, on the other hand, vary over a much wider range. We suspect that at least part of this variability was due to small differences in upper ocean temperature around the floe. For example, the lead adjacent to site 2 was filled with brash during much of the period between day 182 and 190, and it is reasonable to expect that ΔT_w would be lower than at the more open site 1 where the CTD data were taken; a decrease of about 0.24°C in ΔT_w would be needed to increase m_1 to the average of the category 1 values (16×10^{-7}). A small m_1 was also found at site 3 when the water was warm and no brash present. Without brash, there is no obvious reason to believe that m_1 was actually larger. At the opposite extreme were the values calculated during the frontal crossing at sites 1 and 2. There was no evidence of mechanical erosion during this period, and T_w would have to be more than 2°C above the freezing point to explain the departure from the category 1 values. While temperatures during part of the period were actually warmer than this below a depth of 10–15 m, temperatures closer to the ice were always much cooler. This suggests that conditions exist where factors other than ΔT_w are important in determining M_r.

With $m_2 = 1.36$, the best fit to the complete data set was obtained with $m_1 = 30 \times 10^{-7}$, roughly double the category 1 and Mould Bay values. Using the relationship given in (12), we found that nearly 58% of the observed variance in M_r could be explained by ΔT_w. While some of the unexplained

TABLE 4. Lateral Ablation Data Obtained at 5 Sites Near the Drifting Ship *Polarqueen* During MIZEX '84

	Site 1			Site 2		Site 3	Site 4	Site 5
	171–182	182–191	191–193	182–190	190–192	193–198	172–193	190–192
Depth, m								
0.2	0.36	0.47	0.70	0.02	0.33	0.32	1.25	0.22
0.3	0.35	0.42	0.70	0.09	0.23	0.26	1.20	0.14
0.4	0.30	0.40	0.68	0.05	0.26	0.44	1.03	0.16
0.5	0.27	0.30	0.80	0.04	···	0.34	1.02	0.17
0.6	0.27	0.27	0.83	0.03	0.37	0.32	1.00	0.34
0.7	0.25	0.28	0.86	0.10	0.30	0.32	0.90	0.20
0.8	0.23	0.30	0.91	0.08	0.31	0.40	0.80	0.18
0.9	0.23	0.34	0.93	0.07	0.32	0.52	0.76	0.16
1.0	0.23	0.40	1.00	0.10	0.35	0.33	0.76	0.17
$\overline{M_r \Delta t}$, m	0.28	0.35	0.82	0.06	0.31	0.36	0.97	0.19
$\overline{\Delta T_w}$, °C	0.35	0.34	1.12	0.36	0.61	0.86	0.41	0.61
$\bar{u}_*$, m s^{-1}	0.15	0.19	0.23	0.18	0.27	0.16	0.18	0.27
Δt, hours	268	220	50	191	48	120	506	50
$m_1 \times 10^7$	11	18	(39)	(3)	(31)	(9)	(16)	18
$m_1' \times 10^6$	11	16	(17)	(3)	(12)	(5)	(10)	7

Values shown are total ablation measured along the upper meter of the lead walls during the indicated time period (Julian days). Also given are calculated values of m_1 and m_1' for each set of ablation measurements. Parentheses indicate that the value was obtained using CTD data from a different site.

variance is undoubtedly due to uncertainties in ΔT_w, it is likely that part can also be explained by water movement unrelated to local density differences near the lead walls. Externally imposed velocities in the water are closely related to the wind field which produces not only mixing in the lead, but also relative motion between the ice and underlying ocean. Momentum input from the atmosphere to the ocean can be characterized by the friction velocity u_*, the square root of wind stress divided by density. To examine the relationship between M_r and u_*, we initially modified (12) as follows

$$M_r = m_1' u_* \Delta T_w^{m_2} \tag{24}$$

wnere the friction velocity was parameterized by $u_* = C_d^{1/2} u$ and the drag coefficient by $C_d = (0.87 + 0.067u) \times 10^{-3}$ [*Busch*, 1977]. Values of u_* and m_1' are tabulated in Table 4. It can be seen that m_1' exhibits considerably less variability than m_1 and, in particular, that the large coefficients previously found at sites 1 and 2 during the frontal crossing (a period of strong northerly winds and rapid ice drift) are now more in line with the other values. No significant improvement was obtained at site 2 during the first observation period, again suggesting that the inferred ΔT_w was too high. The least squares fit to (24) was obtained with $m_1' = 13.5 \times 10^{-6}$ °C$^{-1.3}$ and $m_2 = 1.3$. The explained variance increased to about 70% with a correlation of 0.85 between observed and calculated values of M_r.

Clearly inclusion of u_* in the BLP improves the prediction of M_r. Although very simple in form, (24) has the undesirable property that $M_r \to 0$ as $u_* \to 0$ and it seems that a more realistic parameterization might take the form, $M_r = (m_1 + m_1' u_*) \Delta T_w^{m_2}$. However, little improvement was obtained when this equation was fit to the data. This was largely a result of an inability to fit the observations at site 1 during the frontal crossing. Neglecting this case produced a drastic decrease in the total variance while increasing the explained variance to about 83% and the correlation between the observed and predicted M_r to 0.92. From the shape of the wall profile, we suspect that the large amount of lateral ablation at site 1 during this period reflects widening of the adjacent lead and entrainment of warmer water from below. This does not appear to have occurred at site 2 or at site 5 where the temperature measurements were made. Uncertainties in T_w obviously impact BLP performance, but other factors such as lead width, current velocity, lead orientation relative to the wind, ice divergence, and F_r may also play a role, especially in regions like the marginal ice zone where there can be large horizontal and vertical gradients in the thermal structure of the upper ocean. We plan to investigate such factors in a more detailed analysis of the MIZEX and Mould Bay data to be presented in a later paper. At this point, however, it appears that the field BLP used in the model calculations provides a reasonable first approximation to M_r throughout much of the Arctic basin. Measurable improvement can be expected if wind data are incorporated into the parameterization, but additional theoretical work and field studies are needed to establish an optimal form.

Discussion

It should be emphasized that the primary focus of this study was on thermodynamic processes related to the interaction of shortwave radiation with the ice-ocean system. This, of course, represents only part of the problem, as dynamic processes in the ice and ocean also affect this interaction. Of concern are many factors which could be of importance during certain times or at particular locations, e.g., entrainment of heat from the deeper ocean, heat exchange between the leads and underlying water, mechanical erosion and floe breakup, spatial variations in lead geometry and ice thickness, meltwater stratification of the upper ocean, and dynamic changes in A_w. While it is beyond the scope of this paper to treat such processes in detail, we would like to make some general comments regarding their relative importance and the utilization of this work in larger-scale models.

In the Arctic basin proper it appears that nearly all of the heat entering the upper ocean is derived from solar radiation

and that F_w is negligible. This is probably not the case in peripheral arctic seas or in the southern ocean where coupled ice-ocean models will be required for accurate predictions of F_w and its effects on the extent and state of the ice cover. Even in these areas, however, F_r is a major factor in the decay cycle whose interaction with the ice and upper ocean is of critical importance in the regional heat and mass balance. MIZEX data suggest that F_{wl} may also be a significant factor in the overall decay pattern, particularly if there are vertical or horizontal temperature gradients in the underlying water. Both upward and downward heat transport seem to take place. Ice divergence during the frontal crossing caused warmer underlying water to be entrained into the leads where it contributed to the rapid disappearance of the brash. Interestingly, the only evidence of this entrainment in the wall profiles was at site 1, and it appears that local geometry must play a role in how this heat affects lateral ablation. Downward advection of water is suggested by changes in the pattern of bottom ablation. When the leads were filled with brash, the average $(dH/dt)_H$ was smaller near the edge of the floe than beneath the interior; however, the pattern reversed once the leads were clear of brash and significant solar heating began to occur. This behavior is consistent with stable water from the leads being forced beneath the surrounding ice. Comparable data are not available from the central Arctic, and we do not yet know to what extent the more stratified upper ocean and lesser dynamic activity might tend to inhibit this exchange. While it is still difficult to establish the magnitude of mixing between the lead and underlying water, the net effect in the stably stratified case will be to divert solar heat from lateral melting into bottom melting, reducing the feedback between F_r and A_w. In cases where the underlying water is warmer than the lead, mixing will increase T_w and dA_w/dt. Vertical exchange between the leads and underlying water can thus affect the relationship between M_r and W and, in the limiting case of complete mixing, would result in bottom and lateral melt rates of comparable size. This is contrary to all field observations, suggesting that F_{wl} is not ordinarily of sufficient magnitude to prevent F_r from making a major contribution to M_r. Nevertheless, this is potentially an important process and additional studies are needed to quantify F_{wl} and its role in the melt cycle.

Dynamic activity affects A_w not only directly but also indirectly by accelerating thermodynamic decay. During MIZEX '84, for example, younger floes were frequently broken up between heavier floes, filling the leads with rapidly melting brash. This process caused the selective removal of first-year ice from the matrix by forcing heat absorbed in the leads to be utilized primarily for the melting of thinner ice. As a result, floes near the edge of the ice pack were predominantly multiyear. In terms of the previous modeling discussion, this process produces, in effect, an ice cover with very small "leads" and very efficient lateral heat transfer to the ice; i.e., T_w remains close to the freezing point, and little energy is lost to the atmosphere. A similar process must also take place during the early part of the melt season in regions of perennial ice. In regions of more uniform ice thickness, floe interactions also result in cracking and continual changes in the floe size distribution [*Rothrock and Thorndike*, 1984]. Because floes increase in number and decrease in average size during the melt progression, it is difficult to establish a general relationship between ice concentration and lead size. For a given value of G_0, we expect that the proportion of lead energy going to lateral melting will increase as total floe perimeter (P_i) in the region increases. There is a direct relation between P_i and the floe size distribution, and it should be possible to include information on floe size distribution in a simple thermodynamic model through P_i. For example, using the BLP in conjunction with data on P_i would allow us to estimate time dependent changes in average lead temperature from (23). A preliminary study of this approach has been made by *Perovich* [1983].

A more complete understanding of the role of F_r in regional ice decay and seasonal mixed layer modifications will require coupled dynamic-thermodynamic simulations with large-scale and mesoscale models. Crucial to the success of such simulations is proper treatment of solar radiation entering the water. Both the IHT and BLP formulations provide substantial improvements over previous methods. The IHT has the advantage that it is independent of lead geometry and can be directly accommodated in existing models. However, we have seen that a large fraction of the heat absorbed in very wide leads is lost to the atmosphere and does not contribute directly to melting. Simpler treatments such as the IHT ignore this loss and tend to become increasingly inaccurate as ice concentration decreases. Although a BLP type formulation overcomes this limitation, its incorporation into a large-scale model is complicated by the nonlinear dependence of lateral melt rate on lead size. The problem this poses is that information on the distribution of open water must somehow be included in the calculations. Simple approaches mentioned above neglect dynamic forcing by winds or currents and are difficult to evaluate owing to lack of suitable data. Summer cloudiness over the polar oceans severely restricts the amount of information available from existing high-resolution satellite imagery, and little is known regarding spatial and temporal changes in the size distribution of leads and floes or about how such changes relate to large scale fields in the atmosphere and ocean. Fortunately, new satellite sensors such as synthetic aparature radar promise to alleviate this situation and provide detailed, all-weather data on ice motion and geometry. Such data will alow the development and testing of much more sophisticated models than are presently possible.

NOTATION

- A_i area covered by ice.
- A_w area covered by open water.
- a subscript referring to atmospheric properties.
- a_1, a_2 empirical coefficients in parameterization of $(1 - \alpha_w)(1 - i_w)$.
- BLP boundary layer parameterization.
- b_1–b_5 empirical coefficients in parameterization of saturation vapor pressure.
- C fractional cloud cover.
- C_e bulk transfer coefficient for latent heat (0.00175).
- C_s bulk transfer coefficient for sensible heat (0.00175).
- c_p specific heat of air at constant pressure (1004 J kg^{-1} °K^{-1}).
- c_w specific heat of water.
- E_w energy content of water column beneath the ice.
- e_s saturation vapor pressure.
- F_c conductive heat flux in the ice.
- F_e latent heat flux.
- F_L flux of incoming long-wave radiation.
- F_m horizontal heat flux at lead edge.

F_{mw} normalized heat flux at floe edge ($F_m H/W$).
F_r flux of incoming shortwave radiation.
F_w heat flux between mixed layer and deeper ocean.
F_{wi} oceanic heat flux at bottom of the ice.
F_{wl} heat flux between lead and underlying water.
G_0 ice concentration.
H ice thickness.
H_0 thickness of surface absorption layer in the ice (0.1 m).
IHT instantaneous heat transfer case.
I_i amount of shortwave radiation transmitted to the ocean through the ice.
I_w amount of shortwave radiation transmitted through the lead and absorbed in the underlying water.
i subscript referring to ice properties.
i_w fraction of net shortwave radiation absorbed below the bottom of the ice.
i_0 fraction of net shortwave radiation that does not contribute directly to surface melting in the ice.
K_e $0.622\ \rho_a L_v C_e/p_0$ (0.468 J m^{-3} mbar^{-1}).
K_s $\rho_a c_p C_s$ (2.28 J m^{-3} °K^{-1}).
L_f latent heat of fusion (0.334 MJ kg^{-1}).
L_v latent heat of vaporazation (2.49 MJ kg^{-1}).
M_r lateral melt rate at floe edge (0.5 dW/dt).
m_1, m_1', m_2 empirical coefficients in boundary layer parameterization.
P_i floe perimeter.
P_w lead perimeter.
p_0 atmospheric pressure at the surface (1013 mbar).
Q_w area integrated input of shortwave radiation to ocean.
q_a specific humidity in air.
q_0 specific humidity at surface.
R rate of energy loss from mixed layer beneath the ice.
r relative humidity.
S_w far field salinity in lead.
T_a air temperature.
T_f salinity determined freezing point temperature.
T_{lim} limiting value of water temperature in a lead.
T_0 ice surface temperature.
T_w far field temperature in lead.
ΔT_w elevation of lead temperature above freezing point ($T_w - T_f$).
t time.
t_d time required for complete decay of ice cover.
u wind speed.
u_* friction velocity.
W lead width.
W_c characteristic lead size.
W_r relaxation width.
w subscript referring to water properties.
Z-L Zubov-Langleben formulation.
α surface albedo.
ε longwave emissivity.
κ bulk extinction coefficient of the ice (1.5 m^{-1}).
ρ density.
σ Stefan-Boltzman constant (5.67×10^{-8} W m^{-2} °K^{-4}).

Acknowledgments. This research was made possible by support from the Office of Naval Research, Arctic Program, under contract N00014-84-C-0111.

REFERENCES

Aagaard, K. L., L. K. Coachman and E. Carmack, On the halocline of the Arctic Ocean, *Deep Sea Res., 28*, 529–545, 1981.

Andreas, E. L., and S. F. Ackley, On the differences in ablation seasons of Arctic and Antarctic sea ice, *J. Atmos. Sci., 39*, 440–447, 1982.

Bulgatov, L. V., and V. F. Zakharov, Heat accumulations in flaw polynyas, *Tr. Arkt. Antarkt. Nauchno. Issled. Inst., 349*, 96–97, 1978.

Busch, N., Fluxes in the surface boundary layer over the sea, in *Modeling and Prediction of the Upper Layer of the Ocean*, edited by E. B. Kraus, pp. 72–91, Pergamon, New York, 1977.

Doronin, Yu. P., and D. E. Kheisin, *Sea Ice* (in Russian), 323 pp., Gidrometeoizdat, Leningrad, 1975. (English translation, National Science Foundation, *Publ. TT75-52088*, Washington, D. C., 1977.

Gast, P. R., Solar radiation, in *Handbook of Geophysics*, edited by C. F. Campen et al., pp. 16-14–16-32, Macmillan, New York, 1960.

Gordon, A. L., Seasonality of southern ocean sea ice, *J. Geophys. Res., 86*, 4193–4197, 1981.

Grenfell, T. C., The effects of ice thickness on the exchange of solar radiation over the polar oceans, *J. Glaciol., 22*, 305–320, 1979.

Grenfell, T. C., and G. A. Maykut, The optical properties of ice and snow in the Arctic basin, *J. Glaciol., 18*(80), 445–463, 1977.

Hornbeck, R. W., *Numerical Methods*, Quantum, New York, 1975.

Idso, S. B., and R. D. Jackson, Thermal radiation from the atmosphere, *J. Geophys. Res., 74*, 5397–5403, 1969.

Josberger, E. G., Laminar and turbulent boundary layers adjacent to melting vertical ice walls in salt water, Ph.D. thesis, 185 pp., Dep. of Oceanogr., Univ. of Wash., Seattle, 1979.

Josberger, E. G., and S. Martin, A laboratory and theoretical study of the boundary layer adjacent to a vertical melting ice wall in salt water, *J. Fluid Mech., 111*, 439–473, 1981.

Langleben, M. P., On the factors affecting the rate of ablation of sea ice, *Can. J. Earth Sci., 3*, 431–439, 1966.

Langleben, M. P., The decay of an annual cover of sea ice, *J. Glaciol., 11*, 337–344, 1972.

Marshunova, M. S., Principal characteristics of the radiation balance of the underlying surface and of the atmosphere in the Arctic, Soviet Data on the Arctic Heat Budget and Its Climatic Influence, *Memo. RM-5003*, edited by J. O. Fletcher et al., pp. 51–131, Rand Corporation, Santa Monica, Calif., 1966.

Maykut, G. A., Energy exchange over young sea ice in the central Arctic, *J. Geophys. Res., 83*, 3646–3658, 1978.

Maykut, G. A., Large-scale heat exchange and ice production in the central Arctic, *J. Geophys. Res., 87*, 7971–7985, 1982.

Maykut, G. A., and P. E. Church, Radiation climate of Barrow, Alaska, 1962–1966, *J. Appl. Meteorol., 12*, 620–628, 1973.

Maykut, G. A., and D. K. Perovich, MIZEX heat and mass balance data, *Rep. APL-UW 12-85*, 73 pp., Appl. Phys. Lab., Univ. of Wash., Seattle, 1985.

Maykut, G. A., and N. Untersteiner, Some results from a time dependent, thermodynamic model of sea ice, *J. Geophys. Res., 76*, 1550–1575, 1971.

Perovich, D. K., On the summer decay of a sea ice cover, Ph.D. dissertation, 176 pp., Geophys. Program, Univ. of Wash., Seattle, 1983.

Rothrock, D. A., and A. S. Thorndike, Measuring the sea ice floe size distribution, *J. Geophys. Res., 89*, 6477–6486, 1984.

Sauberer, F., and I. Dirmhirn, Das Strahlungsklima, in *Klimatographie von Osterreich*, Bd. 3, edited by F. Steinhauser, O. Eckel, and F. Lauscher, pp. 13–102, Österreichische Akademie der Wissenschaften, Vienna, 1958.

Tyler, J. D., and R. C. Smith, *Measurements of Spectral Irradiance Under Water*, 103 pp., Gordon and Breach, New York, 1970.

Zubov, N. N., Arctic Ice (in Russian), 491 pp., Glavsevmorputi, Moscow, 1945. (English translation, U.S. Naval Oceanographic Office, Suitland, Md., 1965.)

G. A. Maykut, Department of Atmospheric Sciences, University of Washington, AK-40, Seattle, WA 98195.

D. K. Perovich, U.S. Army Cold Regions Research and Engineering Laboratory, Hanover, NH 03755.

(Received July 7, 1986;
accepted February 9, 1987.)